

## PDF hosted at the Radboud Repository of the Radboud University Nijmegen

The following full text is a publisher's version.

For additional information about this publication click this link.

<http://hdl.handle.net/2066/155840>

Please be advised that this information was generated on 2020-12-02 and may be subject to change.



# Precise measurement of the top quark mass in dilepton decays using optimized neutrino weighting



D0 Collaboration

V.M. Abazov<sup>af</sup>, B. Abbott<sup>bp</sup>, B.S. Acharya<sup>z</sup>, M. Adams<sup>au</sup>, T. Adams<sup>as</sup>, J.P. Agnew<sup>ap</sup>, G.D. Alexeev<sup>af</sup>, G. Alkhazov<sup>aj</sup>, A. Alton<sup>be,1</sup>, A. Askew<sup>as</sup>, S. Atkins<sup>bc</sup>, K. Augsten<sup>g</sup>, C. Avila<sup>e</sup>, F. Badaud<sup>j</sup>, L. Bagby<sup>at</sup>, B. Baldin<sup>at</sup>, D.V. Bandurin<sup>bv</sup>, S. Banerjee<sup>z</sup>, E. Barberis<sup>bd</sup>, P. Baringer<sup>bb</sup>, J.F. Bartlett<sup>at</sup>, U. Bassler<sup>o</sup>, V. Bazterra<sup>au</sup>, A. Bean<sup>bb</sup>, M. Begalli<sup>b</sup>, L. Bellantoni<sup>at</sup>, S.B. Beri<sup>x</sup>, G. Bernardi<sup>n</sup>, R. Bernhard<sup>t</sup>, I. Bertram<sup>an</sup>, M. Besançon<sup>o</sup>, R. Beuselinck<sup>ao</sup>, P.C. Bhat<sup>at</sup>, S. Bhatia<sup>bg</sup>, V. Bhatnagar<sup>x</sup>, G. Blazey<sup>av</sup>, S. Blessing<sup>as</sup>, K. Bloom<sup>bh</sup>, A. Boehnlein<sup>at</sup>, D. Boline<sup>bm</sup>, E.E. Boos<sup>ah</sup>, G. Borissov<sup>an</sup>, M. Borysova<sup>am,12</sup>, A. Brandt<sup>bs</sup>, O. Brandt<sup>u</sup>, R. Brock<sup>bf</sup>, A. Bross<sup>at</sup>, D. Brown<sup>n</sup>, X.B. Bu<sup>at</sup>, M. Buehler<sup>at</sup>, V. Buescher<sup>v</sup>, V. Bunichev<sup>ah</sup>, S. Burdin<sup>an,2</sup>, C.P. Buszello<sup>al</sup>, E. Camacho-Pérez<sup>ac</sup>, B.C.K. Casey<sup>at</sup>, H. Castilla-Valdez<sup>ac</sup>, S. Caughron<sup>bf</sup>, S. Chakrabarti<sup>bm</sup>, K.M. Chan<sup>az</sup>, A. Chandra<sup>bu</sup>, E. Chapon<sup>o</sup>, G. Chen<sup>bb</sup>, S.W. Cho<sup>ab</sup>, S. Choi<sup>ab</sup>, B. Choudhary<sup>y</sup>, S. Cihangir<sup>at</sup>, D. Claes<sup>bh</sup>, J. Clutter<sup>bb</sup>, M. Cooke<sup>at,11</sup>, W.E. Cooper<sup>at</sup>, M. Corcoran<sup>bu</sup>, F. Couderc<sup>o</sup>, M.-C. Cousinou<sup>l</sup>, J. Cuth<sup>v</sup>, D. Cutts<sup>br</sup>, A. Das<sup>bt</sup>, G. Davies<sup>ao</sup>, S.J. de Jong<sup>ad,ae</sup>, E. De La Cruz-Burelo<sup>ac</sup>, F. Déliot<sup>o</sup>, R. Demina<sup>bl</sup>, D. Denisov<sup>at</sup>, S.P. Denisov<sup>ai</sup>, S. Desai<sup>at</sup>, C. Deterre<sup>ap,3</sup>, K. DeVaughan<sup>bh</sup>, H.T. Diehl<sup>at</sup>, M. Diesburg<sup>at</sup>, P.F. Ding<sup>ap</sup>, A. Dominguez<sup>bh</sup>, A. Dubey<sup>y</sup>, L.V. Dudko<sup>ah</sup>, A. Duperrin<sup>l</sup>, S. Dutt<sup>x</sup>, M. Eads<sup>av</sup>, D. Edmunds<sup>bf</sup>, J. Ellison<sup>ar</sup>, V.D. Elvira<sup>at</sup>, Y. Enari<sup>n</sup>, H. Evans<sup>ax</sup>, A. Evdokimov<sup>au</sup>, V.N. Evdokimov<sup>ai</sup>, A. Fauré<sup>o</sup>, L. Feng<sup>av</sup>, T. Ferbel<sup>bl</sup>, F. Fiedler<sup>v</sup>, F. Filthaut<sup>ad,ae</sup>, W. Fisher<sup>bf</sup>, H.E. Fisk<sup>at</sup>, M. Fortner<sup>av</sup>, H. Fox<sup>an</sup>, S. Fuess<sup>at</sup>, P.H. Garbincius<sup>at</sup>, A. Garcia-Bellido<sup>bl</sup>, J.A. García-González<sup>ac</sup>, V. Gavrilov<sup>ag</sup>, W. Geng<sup>l,bf</sup>, C.E. Gerber<sup>au</sup>, Y. Gershtein<sup>bi</sup>, G. Ginther<sup>at,bl</sup>, O. Gogota<sup>am</sup>, G. Golovanov<sup>af</sup>, P.D. Grannis<sup>bm</sup>, S. Greder<sup>p</sup>, H. Greenlee<sup>at</sup>, G. Grenier<sup>q,r</sup>, Ph. Gris<sup>j</sup>, J.-F. Grivaz<sup>m</sup>, A. Grohsjean<sup>o,3</sup>, S. Grünendahl<sup>at</sup>, M.W. Grünewald<sup>aa</sup>, T. Guillemin<sup>m</sup>, G. Gutierrez<sup>at</sup>, P. Gutierrez<sup>bp</sup>, J. Haley<sup>bq</sup>, L. Han<sup>d</sup>, K. Harder<sup>ap</sup>, A. Harel<sup>bl</sup>, J.M. Hauptman<sup>ba</sup>, J. Hays<sup>ao</sup>, T. Head<sup>ap</sup>, T. Hebbeker<sup>s</sup>, D. Hedin<sup>av</sup>, H. Hegab<sup>bq</sup>, A.P. Heinson<sup>ar</sup>, U. Heintz<sup>br</sup>, C. Hensel<sup>a</sup>, I. Heredia-De La Cruz<sup>ac,4</sup>, K. Herner<sup>at</sup>, G. Hesketh<sup>ap,6</sup>, M.D. Hildreth<sup>az</sup>, R. Hirosky<sup>bv</sup>, T. Hoang<sup>as</sup>, J.D. Hobbs<sup>bm</sup>, B. Hoeneisen<sup>i</sup>, J. Hogan<sup>bu</sup>, M. Hohlfeld<sup>v</sup>, J.L. Holzbauer<sup>bg</sup>, I. Howley<sup>bs</sup>, Z. Hubacek<sup>g,o</sup>, V. Hynek<sup>g</sup>, I. Iashvili<sup>bk</sup>, Y. Ilchenko<sup>bt</sup>, R. Illingworth<sup>at</sup>, A.S. Ito<sup>at</sup>, S. Jabeen<sup>at,13</sup>, M. Jaffré<sup>m</sup>, A. Jayasinghe<sup>bp</sup>, M.S. Jeong<sup>ab</sup>, R. Jesik<sup>ao</sup>, P. Jiang<sup>d</sup>, K. Johns<sup>aq</sup>, E. Johnson<sup>bf</sup>, M. Johnson<sup>at</sup>, A. Jonckheere<sup>at</sup>, P. Jonsson<sup>ao</sup>, J. Joshi<sup>ar</sup>, A.W. Jung<sup>at</sup>, A. Juste<sup>ak</sup>, E. Kajfasz<sup>l</sup>, D. Karmanov<sup>ah</sup>, I. Katsanos<sup>bh</sup>, M. Kaur<sup>x</sup>, R. Kehoe<sup>bt</sup>, S. Kermiche<sup>l</sup>, N. Khalatyan<sup>at</sup>, A. Khanov<sup>bq</sup>, A. Kharchilava<sup>bk</sup>, Y.N. Kharzhev<sup>af</sup>, I. Kiselevich<sup>ag</sup>, J.M. Kohli<sup>x</sup>, A.V. Kozelov<sup>ai</sup>, J. Kraus<sup>bg</sup>, A. Kumar<sup>bk</sup>, A. Kupco<sup>h</sup>, T. Kurča<sup>q,r</sup>, V.A. Kuzmin<sup>ah</sup>, S. Lammers<sup>ax</sup>, P. Lebrun<sup>q,r</sup>, H.S. Lee<sup>ab</sup>, S.W. Lee<sup>ba</sup>, W.M. Lee<sup>at</sup>, X. Lei<sup>aq</sup>, J. Lellouch<sup>n</sup>,

E-mail address: [kehoe@physics.smu.edu](mailto:kehoe@physics.smu.edu) (R. Kehoe).

D. Li<sup>n</sup>, H. Li<sup>bv</sup>, L. Li<sup>ar</sup>, Q.Z. Li<sup>at</sup>, J.K. Lim<sup>ab</sup>, D. Lincoln<sup>at</sup>, J. Linnemann<sup>bf</sup>, V.V. Lipaev<sup>ai</sup>, R. Lipton<sup>at</sup>, H. Liu<sup>bt</sup>, Y. Liu<sup>d</sup>, A. Lobodenko<sup>aj</sup>, M. Lokajicek<sup>h</sup>, R. Lopes de Sa<sup>at</sup>, R. Luna-Garcia<sup>ac,7</sup>, A.L. Lyon<sup>at</sup>, A.K.A. Maciel<sup>a</sup>, R. Madar<sup>t</sup>, R. Magaña-Villalba<sup>ac</sup>, S. Malik<sup>bh</sup>, V.L. Malyshev<sup>af</sup>, J. Mansour<sup>u</sup>, J. Martínez-Ortega<sup>ac</sup>, R. McCarthy<sup>bm</sup>, C.L. McGivern<sup>ap</sup>, M.M. Meijer<sup>ad,ae</sup>, A. Melnitchouk<sup>at</sup>, D. Menezes<sup>av</sup>, P.G. Mercadante<sup>c</sup>, M. Merkin<sup>ah</sup>, A. Meyer<sup>s</sup>, J. Meyer<sup>u,9</sup>, F. Miconi<sup>p</sup>, N.K. Mondal<sup>z</sup>, M. Mulhearn<sup>bv</sup>, E. Nagy<sup>l</sup>, M. Narain<sup>br</sup>, R. Nayyar<sup>aq</sup>, H.A. Neal<sup>be</sup>, J.P. Negret<sup>e</sup>, P. Neustroev<sup>aj</sup>, H.T. Nguyen<sup>bv</sup>, T. Nunnemann<sup>w</sup>, J. Orduna<sup>bu</sup>, N. Osman<sup>l</sup>, J. Osta<sup>az</sup>, A. Pal<sup>bs</sup>, N. Parashar<sup>ay</sup>, V. Parihar<sup>br</sup>, S.K. Park<sup>ab</sup>, R. Partridge<sup>br,5</sup>, N. Parua<sup>ax</sup>, A. Patwa<sup>bn,10</sup>, B. Penning<sup>ao</sup>, M. Perfilov<sup>ah</sup>, Y. Peters<sup>ap</sup>, K. Petridis<sup>ap</sup>, G. Petrillo<sup>bl</sup>, P. Pétrouff<sup>m</sup>, M.-A. Pleier<sup>bn</sup>, V.M. Podstavkov<sup>at</sup>, A.V. Popov<sup>ai</sup>, M. Prewitt<sup>bu</sup>, D. Price<sup>ap</sup>, N. Prokopenko<sup>ai</sup>, J. Qian<sup>be</sup>, A. Quadt<sup>u</sup>, B. Quinn<sup>bg</sup>, P.N. Ratoff<sup>an</sup>, I. Razumov<sup>ai</sup>, I. Ripp-Baudot<sup>p</sup>, F. Rizatdinova<sup>bq</sup>, M. Rominsky<sup>at</sup>, A. Ross<sup>an</sup>, C. Royon<sup>o</sup>, P. Rubinov<sup>at</sup>, R. Ruchti<sup>az</sup>, G. Sajot<sup>k</sup>, A. Sánchez-Hernández<sup>ac</sup>, M.P. Sanders<sup>w</sup>, A.S. Santos<sup>a,8</sup>, G. Savage<sup>at</sup>, M. Savitskyi<sup>am</sup>, L. Sawyer<sup>bc</sup>, T. Scanlon<sup>ao</sup>, R.D. Schamberger<sup>bm</sup>, Y. Scheglov<sup>aj</sup>, H. Schellman<sup>aw</sup>, M. Schott<sup>v</sup>, C. Schwanenberger<sup>ap</sup>, R. Schwienhorst<sup>bf</sup>, J. Sekaric<sup>bb</sup>, H. Severini<sup>bp</sup>, E. Shabalina<sup>u</sup>, V. Shary<sup>o</sup>, S. Shaw<sup>ap</sup>, A.A. Shchukin<sup>ai</sup>, V. Simak<sup>g</sup>, P. Skubic<sup>bp</sup>, P. Slattery<sup>bl</sup>, D. Smirnov<sup>az</sup>, G.R. Snow<sup>bh</sup>, J. Snow<sup>bo</sup>, S. Snyder<sup>bn</sup>, S. Söldner-Rembold<sup>ap</sup>, L. Sonnenschein<sup>s</sup>, K. Soustruznik<sup>f</sup>, J. Stark<sup>k</sup>, D.A. Stoyanova<sup>ai</sup>, M. Strauss<sup>bp</sup>, L. Suter<sup>ap</sup>, P. Svoisky<sup>bp</sup>, M. Titov<sup>o</sup>, V.V. Tokmenin<sup>af</sup>, Y.-T. Tsai<sup>bl</sup>, D. Tsybychev<sup>bm</sup>, B. Tuchming<sup>o</sup>, C. Tully<sup>bj</sup>, L. Uvarov<sup>aj</sup>, S. Uvarov<sup>aj</sup>, S. Uzunyan<sup>av</sup>, R. Van Kooten<sup>ax</sup>, W.M. van Leeuwen<sup>ad</sup>, N. Varelas<sup>au</sup>, E.W. Varnes<sup>aq</sup>, I.A. Vasilyev<sup>ai</sup>, A.Y. Verkhnev<sup>af</sup>, L.S. Vertogradov<sup>af</sup>, M. Verzocchi<sup>at</sup>, M. Vesterinen<sup>ap</sup>, D. Vilanova<sup>o</sup>, P. Vokac<sup>g</sup>, H.D. Wahl<sup>as</sup>, M.H.L.S. Wang<sup>at</sup>, J. Warchol<sup>az</sup>, G. Watts<sup>bw</sup>, M. Wayne<sup>az</sup>, J. Weichert<sup>v</sup>, L. Welty-Rieger<sup>aw</sup>, M.R.J. Williams<sup>ax,14</sup>, G.W. Wilson<sup>bb</sup>, M. Wobisch<sup>bc</sup>, D.R. Wood<sup>bd</sup>, T.R. Wyatt<sup>ap</sup>, Y. Xie<sup>at</sup>, R. Yamada<sup>at</sup>, S. Yang<sup>d</sup>, T. Yasuda<sup>at</sup>, Y.A. Yatsunenko<sup>af</sup>, W. Ye<sup>bm</sup>, Z. Ye<sup>at</sup>, H. Yin<sup>at</sup>, K. Yip<sup>bn</sup>, S.W. Youn<sup>at</sup>, J.M. Yu<sup>be</sup>, J. Zennaro<sup>bk</sup>, T.G. Zhao<sup>ap</sup>, B. Zhou<sup>be</sup>, J. Zhu<sup>be</sup>, M. Zielinski<sup>bl</sup>, D. Zieminska<sup>ax</sup>, L. Zivkovic<sup>n</sup>

<sup>a</sup> LAFEX, Centro Brasileiro de Pesquisas Físicas, Rio de Janeiro, Brazil

<sup>b</sup> Universidade do Estado do Rio de Janeiro, Rio de Janeiro, Brazil

<sup>c</sup> Universidade Federal do ABC, Santo André, Brazil

<sup>d</sup> University of Science and Technology of China, Hefei, People's Republic of China

<sup>e</sup> Universidad de los Andes, Bogotá, Colombia

<sup>f</sup> Charles University, Faculty of Mathematics and Physics, Center for Particle Physics, Prague, Czech Republic

<sup>g</sup> Czech Technical University in Prague, Prague, Czech Republic

<sup>h</sup> Institute of Physics, Academy of Sciences of the Czech Republic, Prague, Czech Republic

<sup>i</sup> Universidad San Francisco de Quito, Quito, Ecuador

<sup>j</sup> LPC, Université Blaise Pascal, CNRS/IN2P3, Clermont, France

<sup>k</sup> LPSC, Université Joseph Fourier Grenoble 1, CNRS/IN2P3, Institut National Polytechnique de Grenoble, Grenoble, France

<sup>l</sup> CPPM, Aix-Marseille Université, CNRS/IN2P3, Marseille, France

<sup>m</sup> LAL, Université Paris-Sud, CNRS/IN2P3, Orsay, France

<sup>n</sup> LPNHE, Universités Paris VI and VII, CNRS/IN2P3, Paris, France

<sup>o</sup> CEA, Irfu, SPP, Saclay, France

<sup>p</sup> IPHC, Université de Strasbourg, CNRS/IN2P3, Strasbourg, France

<sup>q</sup> IPNL, Université Lyon 1, CNRS/IN2P3, Villeurbanne, France

<sup>r</sup> Université de Lyon, Lyon, France

<sup>s</sup> III. Physikalisches Institut A, RWTH Aachen University, Aachen, Germany

<sup>t</sup> Physikalisches Institut, Universität Freiburg, Freiburg, Germany

<sup>u</sup> II. Physikalisches Institut, Georg-August-Universität Göttingen, Göttingen, Germany

<sup>v</sup> Institut für Physik, Universität Mainz, Mainz, Germany

<sup>w</sup> Ludwig-Maximilians-Universität München, München, Germany

<sup>x</sup> Panjab University, Chandigarh, India

<sup>y</sup> Delhi University, Delhi, India

<sup>z</sup> Tata Institute of Fundamental Research, Mumbai, India

<sup>aa</sup> University College Dublin, Dublin, Ireland

<sup>ab</sup> Korea Detector Laboratory, Korea University, Seoul, Republic of Korea

<sup>ac</sup> CINVESTAV, Mexico City, Mexico

<sup>ad</sup> Nikhef, Science Park, Amsterdam, The Netherlands

<sup>ae</sup> Radboud University Nijmegen, Nijmegen, The Netherlands

<sup>af</sup> Joint Institute for Nuclear Research, Dubna, Russia

<sup>ag</sup> Institute for Theoretical and Experimental Physics, Moscow, Russia

<sup>ah</sup> Moscow State University, Moscow, Russia

<sup>ai</sup> Institute for High Energy Physics, Protvino, Russia

<sup>aj</sup> Petersburg Nuclear Physics Institute, St. Petersburg, Russia

<sup>ak</sup> Institució Catalana de Recerca i Estudis Avançats (ICREA) and Institut de Física d'Altes Energies (IFAE), Barcelona, Spain

- <sup>a1</sup> Uppsala University, Uppsala, Sweden  
<sup>am</sup> Taras Shevchenko National University of Kyiv, Kiev, Ukraine  
<sup>an</sup> Lancaster University, Lancaster LA1 4YB, United Kingdom  
<sup>ao</sup> Imperial College London, London SW7 2AZ, United Kingdom  
<sup>ap</sup> The University of Manchester, Manchester M13 9PL, United Kingdom  
<sup>aq</sup> University of Arizona, Tucson, AZ 85721, USA  
<sup>ar</sup> University of California Riverside, Riverside, CA 92521, USA  
<sup>as</sup> Florida State University, Tallahassee, FL 32306, USA  
<sup>at</sup> Fermi National Accelerator Laboratory, Batavia, IL 60510, USA  
<sup>au</sup> University of Illinois at Chicago, Chicago, IL 60607, USA  
<sup>av</sup> Northern Illinois University, DeKalb, IL 60115, USA  
<sup>aw</sup> Northwestern University, Evanston, IL 60208, USA  
<sup>ax</sup> Indiana University, Bloomington, IN 47405, USA  
<sup>ay</sup> Purdue University Calumet, Hammond, IN 46323, USA  
<sup>az</sup> University of Notre Dame, Notre Dame, IN 46556, USA  
<sup>ba</sup> Iowa State University, Ames, IA 50011, USA  
<sup>bb</sup> University of Kansas, Lawrence, KS 66045, USA  
<sup>bc</sup> Louisiana Tech University, Ruston, LA 71272, USA  
<sup>bd</sup> Northeastern University, Boston, MA 02115, USA  
<sup>be</sup> University of Michigan, Ann Arbor, MI 48109, USA  
<sup>bf</sup> Michigan State University, East Lansing, MI 48824, USA  
<sup>bg</sup> University of Mississippi, University, MS 38677, USA  
<sup>bh</sup> University of Nebraska, Lincoln, NE 68588, USA  
<sup>bi</sup> Rutgers University, Piscataway, NJ 08855, USA  
<sup>bj</sup> Princeton University, Princeton, NJ 08544, USA  
<sup>bk</sup> State University of New York, Buffalo, NY 14260, USA  
<sup>bl</sup> University of Rochester, Rochester, NY 14627, USA  
<sup>bm</sup> State University of New York, Stony Brook, NY 11794, USA  
<sup>bn</sup> Brookhaven National Laboratory, Upton, NY 11973, USA  
<sup>bo</sup> Langston University, Langston, OK 73050, USA  
<sup>bp</sup> University of Oklahoma, Norman, OK 73019, USA  
<sup>bq</sup> Oklahoma State University, Stillwater, OK 74078, USA  
<sup>br</sup> Brown University, Providence, RI 02912, USA  
<sup>bs</sup> University of Texas, Arlington, TX 76019, USA  
<sup>bt</sup> Southern Methodist University, Dallas, TX 75275, USA  
<sup>bu</sup> Rice University, Houston, TX 77005, USA  
<sup>bv</sup> University of Virginia, Charlottesville, VA 22904, USA  
<sup>bw</sup> University of Washington, Seattle, WA 98195, USA

## ARTICLE INFO

## Article history:

Received 13 August 2015

Received in revised form 19 October 2015

Accepted 31 October 2015

Available online 11 November 2015

Editor: H. Weerts

## ABSTRACT

We measure the top quark mass in dilepton final states of  $t\bar{t}$  events in  $p\bar{p}$  collisions at  $\sqrt{s} = 1.96$  TeV, using data corresponding to an integrated luminosity of  $9.7 \text{ fb}^{-1}$  at the Fermilab Tevatron Collider. The analysis features a comprehensive optimization of the neutrino weighting method to minimize the statistical uncertainties. We also improve the calibration of jet energies using the calibration determined in  $t\bar{t} \rightarrow \text{lepton} + \text{jets}$  events, which reduces the otherwise limiting systematic uncertainty from the jet energy scale. The measured top quark mass is  $m_t = 173.32 \pm 1.36(\text{stat}) \pm 0.85(\text{syst})$  GeV.

© 2015 The Authors. Published by Elsevier B.V. This is an open access article under the CC BY license (<http://creativecommons.org/licenses/by/4.0/>). Funded by SCOAP<sup>3</sup>.

## 1. Introduction

The discovery of the top quark in 1995 [1,2] completed the three quark families of the standard model (SM). Since then, the top quark has been one of the focal points of the Fermilab Tevatron and of the CERN LHC programs. The top quark stands out because of its large mass,  $m_t$ , which is a fundamental parameter in the SM. Its Yukawa coupling to the Higgs boson,  $Y_t = \sqrt{2}m_t/v$ , where  $v$  is the vacuum expectation value of the Higgs field, is close to unity, implying that the top quark may play a special role in electroweak symmetry breaking. In addition,  $m_t$  is linked to the  $W$  and Higgs boson masses,  $M_W$  and  $M_H$ , through radiative corrections [3]. Following the Higgs boson discovery [4,5], a precise measurement of  $m_t$  provides a test of the electroweak sector of the SM and information on whether our universe resides in a stable or metastable region of that theory [6–8]. The short lifetime of the top quark prevents its confinement in the strong color field, since top quarks decay before hadronizing. This allows a particularly precise study of pure quantum chromodynamic (QCD) effects. A comparison of the measured  $m_t$  and the  $m_t$  extracted from cross section mea-

<sup>1</sup> Visitor from Augustana College, Sioux Falls, SD, USA.

<sup>2</sup> Visitor from The University of Liverpool, Liverpool, UK.

<sup>3</sup> Visitor from DESY, Hamburg, Germany.

<sup>4</sup> Visitor from CONACyT, Mexico City, Mexico.

<sup>5</sup> Visitor from SLAC, Menlo Park, CA, USA.

<sup>6</sup> Visitor from University College London, London, UK.

<sup>7</sup> Visitor from Centro de Investigacion en Computacion – IPN, Mexico City, Mexico.

<sup>8</sup> Visitor from Universidade Estadual Paulista, São Paulo, Brazil.

<sup>9</sup> Visitor from Karlsruhe Institut für Technologie (KIT) – Steinbuch Centre for Computing (SCC), D-76128 Karlsruhe, Germany.

<sup>10</sup> Visitor from Office of Science, U.S. Department of Energy, Washington, D.C. 20585, USA.

<sup>11</sup> Visitor from American Association for the Advancement of Science, Washington, D.C. 20005, USA.

<sup>12</sup> Visitor from Kiev Institute for Nuclear Research, Kiev, Ukraine.

<sup>13</sup> Visitor from University of Maryland, College Park, Maryland 20742, USA.

<sup>14</sup> Visitor from European Organization for Nuclear Research (CERN), Geneva, Switzerland.

measurements [9–12] may provide a probe of higher order and soft QCD corrections to the observed mass [13].

Assuming the SM branching ratio of  $t \rightarrow Wb \approx 100\%$ ,  $t\bar{t}$  decays yield distinct final state categories according to the number of charged leptons with high transverse momentum ( $p_T$ ) from  $W$  boson decays. Dilepton ( $2\ell$ ,  $\ell = e$  or  $\mu$ ) events, such as  $ee$ ,  $e\mu$ , and  $\mu\mu$ , with neutrinos from two  $W \rightarrow \ell\nu$  decays, are relatively rare but have low background. We present a measurement of  $m_t$  using  $p\bar{p}$  collider data collected with the D0 detector at the Fermilab Tevatron collider, corresponding to an integrated luminosity of  $9.7 \text{ fb}^{-1}$ , in events with two high- $p_T$  electrons or muons of opposite electric charge. Two high- $p_T$  jets must also be observed, one of which must be identified as being consistent with originating from a  $b$  quark. This analysis is based on our previous dilepton measurement [14], but with increased integrated luminosity and multiple optimizations to improve the precision of  $m_t$ . We reduce the dominant statistical contribution to the uncertainty on  $m_t$  through an optimization of the methods for kinematic reconstruction and statistical analysis. Lacking a dijet signature from  $W \rightarrow q\bar{q}'$ , which is present in  $t\bar{t} \rightarrow \text{lepton} + \text{jets}$  ( $\ell + \text{jets}$ ) events and was used to improve the precision of jet energy calibration with a  $W$  mass constraint [15], previous dilepton analyses at the Tevatron have reached a sensitivity limit imposed by standard jet calibration methods [16,17]. Progress in calibrating jet energies in the dilepton channel [14] provides improved cross-checks across different channels and a more significant contribution from the dilepton channel to the world average  $m_t$  [18]. For comparison, the most recent measurements of  $m_t$  in the dilepton channel from CDF, ATLAS, and CMS are, respectively,  $m_t = 171.5 \pm 1.9(\text{stat}) \pm 2.5(\text{syst}) \text{ GeV}$  [19],  $m_t = 173.79 \pm 0.54(\text{stat}) \pm 1.30(\text{syst}) \text{ GeV}$  [20], and  $m_t = 172.50 \pm 0.43(\text{stat}) \pm 1.46(\text{syst}) \text{ GeV}$  [21]. In this analysis, we substantially reduce the otherwise dominant uncertainty in the jet energy scale by applying the methods of Ref. [14].

## 2. Detector and data sample

### 2.1. Detector

The D0 detector [22,23] has a central-tracking system, consisting of a silicon microstrip tracker and a central fiber tracker, both located within a 1.9 T superconducting solenoidal magnet, with designs optimized for identification of the  $p\bar{p}$  collision vertex and track reconstruction at pseudorapidities [24] of  $|\eta| < 3$  and  $|\eta| < 2.5$ , respectively. The liquid-argon/uranium calorimeter has a central section covering  $|\eta| \leq 1.1$ , and two end sections that extend coverage to  $|\eta| \approx 4.2$ , with all three housed in separate cryostats. An outer muon system, covering  $|\eta| < 2$ , consists of a layer of tracking detectors and scintillation trigger counters in front of 1.8 T iron toroids, followed by two similar layers after the toroids.

### 2.2. Object reconstruction

We require electrons to satisfy an identification criterion based on boosted decision trees [25] using calorimeter and tracking information. Muons must satisfy requirements that match hits in the muon system to a track in the central tracking detector that is required to have a small distance of closest approach to the beam axis [26]. We require hits in the muon layers inside and outside the toroid. Muons and charged hadron momenta are measured in the central tracking detector, while electron, photon ( $\gamma$ ), jet, and charged hadron energies are measured in the calorimeters. Muons must be isolated from jets and from nearby tracks. Electrons and muons must have their extrapolated track trajectories isolated from calorimeter energy depositions greater than an energy threshold. Electrons and muons must have  $p_T > 15 \text{ GeV}$ ,

and  $|\eta| < 2.5$  and  $< 2.0$ , respectively. We reconstruct jets using an iterative, midpoint-seeded cone algorithm with a cone parameter of  $\mathcal{R}_{\text{cone}} = 0.5$  [27]. Jets with embedded muons from the decay of  $b$ -hadrons require an additional correction to jet energy to account for the associated neutrino. A multivariate discriminant [28] is used to identify jets that contain a  $b$ -hadron (i.e.,  $b$  jets) from a vertex displaced from the interaction point. We define the missing transverse momentum ( $\cancel{E}_T$ ) attributed to the escaping neutrinos as the negative of the vector sum of all transverse components of calorimeter cell energies, corrected for the measured muon momenta and the response of the calorimeter to electrons. We also correct  $\cancel{E}_T$  for detector response in the jet energy calibration, as described below. Details of object reconstruction are provided in Ref. [29].

### 2.3. Standard jet energy calibration

We calibrate the energy of jets to be the energy of the particle jets reconstructed using the midpoint algorithm [27]. We correct for the effects of the calorimeter response to particle constituents of jets, energy leaking into the cone from particles directed outside it, as well as energy deposits outside the cone from particles inside it [30]. Charged hadrons have an energy-dependent response that is lower than that of electrons and photons. We therefore apply corrections obtained from  $\gamma + \text{jet}$  events to account for the energy dependence of the jet response in the central  $|\eta|$  region. We also apply a relative  $\eta$ -dependent correction obtained from  $\gamma + \text{jet}$  and dijet events. We employ the same methods to calibrate jet energies independently in the Monte Carlo (MC) simulation and in data. The MC is used to help study potential biases in the data. We incorporate a correction for jets in the MC simulation that accounts for the difference in single-particle response between data and MC. This procedure ensures that the flavor dependence of the jet response in data is replicated in MC. In the MC we account for multiple  $p\bar{p}$  interactions by correcting the jet energy to the particle level of only those particles that are directed within the jet cone at particle level. The typical systematic uncertainty in the energy calibration of each jet in the dilepton sample is 2%. This precision is limited by systematic uncertainties of the  $\gamma + \text{jet}$  method in the  $p_T$  range of jets in  $t\bar{t}$  events. Details about this “standard jet energy scale” calibration can be found in Ref. [30]. We require that jets have  $p_T > 20 \text{ GeV}$  and  $|\eta| < 2.5$  after calibration, but before applying additional corrections from the  $W \rightarrow q\bar{q}'$  constraint in the  $\ell + \text{jets}$  channel discussed below.

## 3. Absolute jet calibration from a $W \rightarrow q\bar{q}'$ constraint

As in Ref. [14], we apply a multiplicative correction factor to the energy of jets in data based on an analysis of  $t\bar{t} \rightarrow \ell + \text{jets}$  events using the  $W \rightarrow q\bar{q}'$  decays as a constraint. Application of this factor,  $1.0250 \pm 0.0046(\text{stat})$  [15], improves the agreement between MC and data and allows us to use its uncertainty to reduce the uncertainty on the absolute energy scale by a factor of  $\approx 4$  relative to the standard jet energy scale, while retaining its  $\eta$  and  $p_T$  dependence. To apply this scale, which comes from light-quark jets, to the dilepton sample, which has  $b$  jets, it is important to ensure that the variation in the ratio of data over MC jet response between different flavors be placed on an equal footing. The standard jet energy scale [30] achieves this on a jet-by-jet basis by using single particles in MC jets to correct the simulation so that it has the same kinematic and flavor-dependent jet response as that in data. This ensures that the energies of  $b$  jets in dilepton simulated samples agree with those of  $b$  jets in the dilepton data sample at the same level as light-quark jets. Aside from fragmentation differences between data and MC which are discussed below, this

approach justifies the use of the  $\ell + \text{jets}$  constraint in the dilepton channel.

#### 4. Event selection

The  $t\bar{t}$  candidate events in the  $ee$  and  $\mu\mu$  channels are required to pass single-lepton triggers. The full suite of triggers is used for selecting  $e\mu$  events. The dilepton event selection before optimization is described in Ref. [29]. We optimize the selection based on MC events to provide the smallest expected statistical uncertainty in  $m_t$ . We require two isolated leptons with opposite electric charge. We require at least two jets, where at least one of the two jets with highest  $p_T$  must be identified as a  $b$  jet. For the  $e\mu$  channel, our selections have an efficiency for tagging  $b$  jets of 72%, and a light-quark mistag rate of 12% in the central region in  $\eta$ . The same-flavor channels employ slightly tighter  $b$  tagging requirements and thus have a few percent lower efficiency, and 30% lower mistag rate. We require events in the  $\mu\mu$  channel to have  $\cancel{E}_T > 40$  GeV. This  $\cancel{E}_T$  selection is also applied to  $ee$  events when the dielectron invariant mass is between 70 and 100 GeV, to reduce the  $Z \rightarrow ee$  background contribution. We define a  $\cancel{E}_T$  significance variable,  $S$ , which measures the likelihood for the observed  $\cancel{E}_T$  to be a fluctuation from  $\cancel{E}_T = 0$  GeV. We require  $S > 3.5$  (4) for the  $ee$  ( $\mu\mu$ ) channel. We require  $e\mu$  events to have  $H_T > 100$  GeV, where  $H_T$  is the scalar sum of the  $p_T$  of the two highest- $p_T$  jets and of the lepton with highest  $p_T$ . The  $H_T$ ,  $b$  tagging, and  $\cancel{E}_T$ -based requirements are optimized to minimize the expected statistical uncertainty on  $m_t$  in each channel. The expected signal-to-background (S/B) ratio is  $\approx 7$  for these channels. These requirements yield a 3% improvement in statistical precision in  $m_t$  relative to the selections in Ref. [14]. After implementing all these selections, we obtain 340, 115, and 110 events in the  $e\mu$ ,  $ee$  and  $\mu\mu$  channels, respectively.

#### 5. Modeling signal and background

The  $t\bar{t}$  events are simulated at 15 mass points over the range  $130 \leq m_t^{\text{MC}} \leq 200$  GeV using the tree level generator ALPGEN 2.11 [31] with up to 2 additional light partons and PYTHIA 6.409 [32] with modified underlying event Tune A for parton showering and hadronization. Here,  $m_t^{\text{MC}}$  refers to the input mass in ALPGEN. An additional, larger sample is generated at  $m_t^{\text{MC}} = 172.5$  GeV to study systematic uncertainties. We normalize the  $t\bar{t}$  production cross section to  $\sigma_{t\bar{t}} = 7.24 \pm 0.23$  pb [33], which is calculated at next-to-next-to-leading order with a next-to-next-to-leading logarithm soft gluon resummation. The main backgrounds arise from three sources:  $Z/\gamma^* \rightarrow \ell^+\ell^-$ , diboson ( $WW$ ,  $WZ$ , and  $ZZ$ ) processes, and instrumental effects. We model the  $Z/\gamma^*$  background using ALPGEN with up to 2 light partons and PYTHIA for showering and hadronization. We employ PYTHIA for the diboson background. The instrumental background arises from  $W + \text{jets}$ , multijet, or  $\ell + \text{jets}$   $t\bar{t}$  events where one or two jets are either mis-identified as electrons, or they contain a hadron decaying to a non-isolated lepton that passes our selection. This background is estimated from data as in Ref. [29]. We apply a full detector simulation based on GEANT 3.14 [34] for all simulated events. The objects reconstructed in simulation are smeared to ensure that their resolutions reflect those in data. Scale factors in object efficiencies are applied to improve agreement between data and MC.

#### 6. Kinematic reconstruction

##### 6.1. Neutrino weighting

The presence of two neutrinos in the  $t\bar{t}$  decay makes it impossible to fully constrain the kinematics and thus extract a unique  $m_t$

measurement from each event. Given the measured momenta of leptons, jets and  $\cancel{E}_T$ , the available constraints from  $M_W$ , and the condition  $m_t = m_{\bar{t}}$ , we are missing one constraint to provide full  $t\bar{t}$  reconstruction in dilepton events. We integrate over the phase space of neutrino rapidities for chosen values of hypothesized  $m_t$  ( $m_t^h$ ) [35], and compare  $\cancel{E}_T^{\text{calc}}$ , the vector sum of neutrino momentum solutions at each chosen point of phase space, to the observed  $\cancel{E}_T^{\text{obs}}$  to determine a “weight”  $\omega$  characterizing the level of agreement:

$$\omega = \frac{1}{N} \sum_{i=1}^N \prod_{j=x,y} \exp\left(-\frac{(\cancel{E}_{j,i}^{\text{calc}} - \cancel{E}_j^{\text{obs}})^2}{2\sigma_{\cancel{E}_T}^2}\right), \quad (1)$$

where  $i$  runs over all neutrino solutions for any two possible jet-lepton assignments in the  $t\bar{t}$  final state (up to  $N = 8$ ),  $j$  stands for the two orthogonal coordinates in the transverse plane ( $x$  and  $y$ ), and  $\sigma_{\cancel{E}_T}$  is a parameter representing the RMS of the difference between the transverse components of the measured  $\cancel{E}_T$  and the sum of the solved neutrino transverse momenta. The parameter  $\sigma_{\cancel{E}_T}$  is taken to be the same in both  $x$  and  $y$  directions. We perform this calculation over a range of  $m_t^h$ , integrating  $\omega$  over the neutrino phase space, to yield a distribution of  $\omega(m_t)$  versus  $m_t^h$ . Prior studies [36] have shown that the first two moments ( $\mu_\omega, \sigma_\omega$ ) of this distribution extract most of the information about  $m_t$ . The analysis of Ref. [14] used the range of  $m_t^h$  values between 80 and 330 GeV in 1 GeV steps and a  $\sigma_{\cancel{E}_T}$  of 7 GeV in the weight calculation. The new optimized determination of these parameters is briefly summarized below.

##### 6.2. Optimization of weight calculation parameters

After applying the methods described above to improve the jet energy calibration, the statistical contribution is the dominant source of measurement uncertainty on  $m_t$  in the dilepton channel. We therefore examine the parameters used for the kinematic reconstruction of  $t\bar{t}$  events and for the maximum likelihood fit to reduce the expected statistical uncertainty. At each step, we verify through MC simulations that the optimization does not increase the systematic uncertainty.

All neutrino solutions and jet assignments yield mass estimators such as  $\mu_\omega$  that are correlated with  $m_t$ . However, the correlation is substantially greater, and  $\mu_\omega$  values are less biased, when the correct jet assignments and solutions of neutrino momenta are chosen. Since now  $m_t$  has been measured with high precision [18], we can optimize the range of  $m_t^h$  based on known values of  $m_t$ . Considering a wide range in  $m_t^h$  causes incorrect configurations to overwhelm the correct configuration, thereby worsening the mass resolution. Likewise, scanning over too narrow a range biases the background and worsens the mass sensitivity by causing  $t\bar{t}$  and background distributions to be similar. Examination of a two-dimensional grid of upper and lower limits of the mass range yields the optimal range of  $m_t^h = 115$  to 220 GeV in 1 GeV steps. The value of  $\sigma_{\cancel{E}_T}$  also has a noticeable impact on the expected precision of the analysis. This was not the case in Ref. [14], mainly because the final top quark mass measurement was less precise. In Ref. [14], the value of 7 GeV for  $\sigma_{\cancel{E}_T}$  was obtained as the unclustered  $\cancel{E}_T$  resolution in an earlier dataset [36], where the unclustered  $\cancel{E}_T$  is the magnitude of the vector sum of all energy depositions in the calorimeter that are not included in lepton or jet reconstruction. However, accounting only for the unclustered energy resolution as the origin of the difference between the calculated and measured  $\cancel{E}_T$  ignores the effect of assumptions that go into the kinematic reconstruction. For instance, the finite binning of the neutrino rapidities discretizes the solved neutrino momenta and therefore the solved  $\cancel{E}_T$ . Also, the solved  $\cancel{E}_T$  does not include

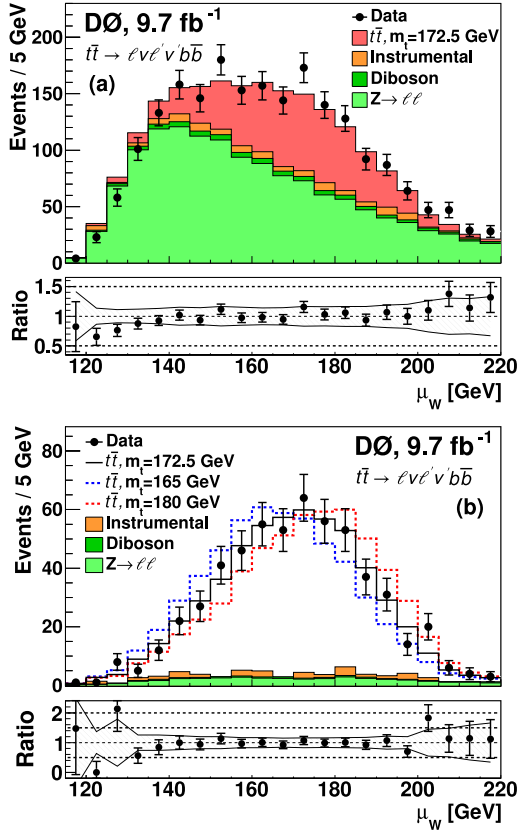


**Fig. 1.** The distribution in the mass estimator,  $\mu_w$ , for the combination of the  $ee$ ,  $e\mu$ , and  $\mu\mu$  channels for (a) the preselected sample and (b) the final event sample. The MC events are normalized separately to the number of observed events in data in each channel. The ratios show the total number of observed events divided by the number of expected events in a given bin of  $\mu_w$  for  $m_t^{\text{MC}} = 172.5$  GeV. The band of systematic uncertainty is shown as the shaded area in the ratio plots, which includes contributions from the dominant sources: jet energy scale, lepton identification, lepton momentum scale, luminosity,  $b$  quark modeling, initial and final state radiation, color reconnection, as well as hadronization and higher-order QCD effects for  $t\bar{t}$  events.

additional jets, reconstructed or not, since only the two leading jets are considered in the kinematic reconstruction. Due to these additional contributions, a scan in a wide range from 7 to 100 GeV is performed and we find the optimal value for  $\sigma_{\vec{E}_T}$  to be 25 GeV, which is larger than the 7 GeV of Ref. [14]. Combined, these optimizations improve the expected combined statistical uncertainty on  $m_t$  by 11% compared to the parameters in Ref. [14].

### 6.3. Efficiency of kinematic reconstruction and event yields

Events used in the analysis must have at least one pair of neutrino solutions for at least one  $m_t^h$  value. The efficiency for this kinematic reconstruction is over 99% for  $t\bar{t}$  events, and 91% to 98% for the background. In the final sample, a total of 336, 113, and 109 events in the  $e\mu$ ,  $ee$ , and  $\mu\mu$  channels, respectively, pass the kinematic reconstruction. The expected sum of  $t\bar{t}$  and background yields and their corresponding asymmetric total uncertainties (stat  $\oplus$  syst) are  $298.1^{+22.1}_{-27.2}$ ,  $106.5^{+10.4}_{-11.6}$ , and  $103.5^{+7.4}_{-9.1}$  events for the  $e\mu$ ,  $ee$ , and  $\mu\mu$  channels, respectively. The distributions of the mass estimator  $\mu_\omega$  in a preselected sample, omitting requirements on  $b$  tagging,  $\cancel{E}_T$ ,  $\cancel{E}_T$  significance, and  $H_T$ , are shown in Fig. 1(a). The  $t\bar{t}$  component is evident in the preselected data. The mass dependence of the  $\mu_\omega$  distribution is given in Fig. 1(b) for three  $m_t^{\text{MC}}$  mass points with all selections applied.

## 7. Extracting the top quark mass

### 7.1. Maximum likelihood

We perform a binned maximum likelihood fit to the extracted moment distributions  $[\mu_\omega, \sigma_\omega]$  in data. Expected probability densities are calculated using the MC samples for each of the 16  $m_t$  points, yielding a two-dimensional probability density  $h_S(\mu_\omega, \sigma_\omega | m_t^{\text{MC}})$  distribution parametrized by  $m_t$ . Background samples are used to construct a background template for each channel,  $h_B(\mu_\omega, \sigma_\omega)$ , with each background contributing according to its expected yield. Bins in signal templates with no events are given a weighted value corresponding to a single signal MC event to ensure that the log of likelihood is not infinite. The likelihood is given by:

$$\mathcal{L}(\mu_\omega\{1..N\}, \sigma_\omega\{1..N\}, N | n_S, n_B, m_t) = \prod_{i=1}^N \frac{n_S \cdot h_S(\mu_{\omega i}, \sigma_{\omega i} | m_t) + n_B \cdot h_B(\mu_{\omega i}, \sigma_{\omega i})}{n_S + n_B}, \quad (2)$$

where  $N$  is the number of observed events in data,  $n_S$  is the expected number of  $t\bar{t}$  events (for  $m_t = 172.5$  GeV), and  $n_B$  is the expected total number of background events. We fit  $(-\ln \mathcal{L})$  versus  $m_t^{\text{MC}}$  to a parabola in a window of  $m_t^{\text{MC}}$  that is iteratively varied until a stable minimum is found. We take the minimum of the final parabola to be the fitted top quark mass,  $m_t^{\text{fit}}$ . The uncertainty on the fitted mass is obtained by considering the  $m_t^{\text{MC}}$  range over which the fit function increases by 0.5 units in  $(-\ln \mathcal{L})$  above this minimum. Using pseudo-experiments, we optimize the template binning of each channel separately in a two-dimensional grid that lets  $\mu_\omega$  and  $\sigma_\omega$  bin sizes vary independently. Finer binning in  $\mu_\omega$  and  $\sigma_\omega$ , especially for the  $e\mu$  channel, improves the expected statistical precision in  $m_t^{\text{fit}}$  by 5%. The fitted mass window is optimized to  $\pm 15$  GeV for all channels. Taking all the optimizations together, including event selection, weight calculation, and maximum likelihood fitting, the statistical sensitivity of this analysis is improved relative to Ref. [14] by 20% beyond the 35% gain expected from increased integrated luminosity.

### 7.2. Ensemble testing and data results

We obtain a linear relationship between  $m_t^{\text{fit}}$  and  $m_t^{\text{MC}}$  by performing randomized pseudo-experiments using all signal mass points. The numbers of signal and background events in the pseudo-experiments are allowed to fluctuate within their Poisson uncertainties around their expected values. We require that the total number of events matches that observed in data. To minimize the effect of statistical fluctuations on our systematic uncertainties, we optimize the number of pseudo-experiments by dividing the MC sample into five subsamples, and measure systematic uncertainties with each subsample. We calculate the RMS of the five uncertainties, average over all systematic effects, and divide by  $\sqrt{5}$  to estimate the statistical component of systematic uncertainties. The average RMS decreases until we oversample, or reuse, the  $t\bar{t}$  MC events by roughly a factor of three. This corresponds to 3000 pseudo-experiments. We perform a linear fit of  $m_t^{\text{fit}}$  versus  $m_t^{\text{MC}}$  to obtain a calibration slope and offset for  $m_t^{\text{fit}}$  using 3000 pseudo-experiments:

$$m_t^{\text{fit}} = \text{Slope} \cdot (m_t^{\text{MC}} - 170) + \text{Offset} + 170. \quad (3)$$

We account for oversampling by increasing the statistical uncertainties at each mass point by the appropriate oversampling factor. Likewise, we compute the pull, or the ratio of  $m_t^{\text{fit}} - m_t^{\text{MC}}$  over the average estimated uncertainty at each mass point. The slopes

**Table 1**

Slopes, offsets, and pull widths of the  $m_t$  calibration and the expected statistical uncertainties in the mass ( $\sigma_{m_t}$ ) for the  $ee$ ,  $e\mu$ , and  $\mu\mu$  channels, and their combination.

	Slope	Offset [GeV]	Pull width	$\sigma_{m_t}$ [GeV]
$ee$	$0.984 \pm 0.004$	$0.671 \pm 0.043$	0.994	2.98
$e\mu$	$0.986 \pm 0.006$	$0.548 \pm 0.065$	0.998	1.72
$\mu\mu$	$0.989 \pm 0.010$	$0.717 \pm 0.103$	1.004	3.31
$2\ell$	$0.988 \pm 0.006$	$0.617 \pm 0.063$	0.995	1.35

**Table 2**

Systematic uncertainties on  $m_t$  for the combined dilepton measurement using  $9.7 \text{ fb}^{-1}$  of integrated luminosity. For symmetrized uncertainties, the “ $\pm$ ” symbol indicates that the corresponding systematic parameters in MC are positively correlated with  $m_t$  in data, and the “ $\mp$ ” symbol indicates an anticorrelation. The uncertainties shown as + or – only are computed by comparing a standard choice with an alternate, but are symmetrized in calculating the total uncertainty.

Source	$\sigma_{m_t}$ [GeV]
Jet energy calibration	
Absolute scale	$\mp 0.47$
Flavor dependence	$\mp 0.27$
Residual scale	$+0.36$
$b$ quark fragmentation	$-0.35$
	$+0.10$
Object reconstruction	
Trigger	$-0.06$
Electron $p_T$ resolution	$\pm 0.01$
Muon $p_T$ resolution	$\mp 0.03$
Electron energy scale	$\pm 0.01$
Muon $p_T$ scale	$\pm 0.01$
Jet resolution	$\mp 0.12$
Jet identification	$+0.03$
$b$ tagging	$\mp 0.19$
Signal modeling	
Higher-order effects	$-0.33$
ISR/FSR	$\pm 0.15$
$p_T(t\bar{t})$	$-0.07$
Hadronization	$-0.11$
Color reconnection	$-0.22$
Multiple $p\bar{p}$ interactions	$-0.06$
PDF uncertainty	$\pm 0.08$
Background modeling	
Signal fraction	$\pm 0.01$
Heavy-flavor scale factor	$\pm 0.04$
Method	
Template statistics	$\pm 0.18$
Calibration	$\pm 0.07$
Total systematic uncertainty	$\pm 0.85$

of  $m_t^{\text{fit}}$  versus  $m_t^{\text{MC}}$  are close to 1, and pull widths are consistent with unity, as shown in Table 1. We calculate the final  $m_t$  by correcting  $m_t^{\text{fit}}$  from a given measurement by the slope and offset. We correct the statistical uncertainty using the slope and the pull width. The expected corrected statistical uncertainties for each channel are given in Table 1. In data, we obtain corrected, fitted  $m_t$  values of  $m_t = 171.86 \pm 1.71(\text{stat})$ ,  $173.99 \pm 3.04(\text{stat})$ , and  $178.58 \pm 3.56(\text{stat})$  GeV for the  $e\mu$ ,  $ee$ , and  $\mu\mu$  channels respectively, and  $m_t = 173.32 \pm 1.36(\text{stat})$  GeV for the combined channels.

## 8. Systematic uncertainties

Systematic uncertainties summarized in Table 2 arise from jet energy calibration, object reconstruction, modeling of  $t\bar{t}$  and background events, and the mass-extraction method. The energies of jets are shifted up and down by the uncertainty on the absolute energy scale, which is taken from  $\ell + \text{jets}$  events, thereby providing shifts in  $m_t$ . This scale is appropriate for light-quark jets, which, after correcting for jet flavors to improve the agreement

between data and MC, have different kinematic distributions than  $b$  jets from  $t\bar{t}$  decays. We calculate a residual uncertainty due to the kinematic differences between the  $\ell + \text{jets}$  calibration sample and dilepton sample of  $b$  jets. We use separate up and down estimates to extract the energy- and  $\eta$ -dependent shifts in  $m_t$  based on uncertainties in the standard jet energy scale relative to their average value in the  $\ell + \text{jets}$  calibration sample. We cross-check this with an alternative method that applies shifted light-quark jet energy scales to  $b$  jets in the  $\ell + \text{jets}$  channel [15]. These methods agree, and thereby validate the use of the  $\ell + \text{jets}$  scale as a jet calibration. We also cross-check using a jet-energy-dependent linear parameterization of the residual jet energy scale as in Ref. [15], obtaining results that do not exceed our estimate of uncertainties from the jet energy scale. To estimate the uncertainty corresponding to possible differences in the flavor dependence of the MC scale relative to data, we change the single-particle responses up and down by their uncertainties and obtain the shift in  $m_t$ . To estimate the possible dependence on the  $b$  quark fragmentation in the MC, we replace the PYTHIA  $b$  quark fragmentation function with the Bowler scheme [37], and compare  $m_t$  with the Bowler free parameters tuned to LEP (ALEPH, OPAL, and DELPHI) or SLD data [38].

The systematic uncertainty due to the trigger efficiency is estimated by applying the ratio of single lepton trigger efficiency parameterization in data divided by the MC parameterization to the  $ee$  and  $\mu\mu$  channels. The uncertainties in the modeling of the energy and momentum resolutions of electrons, muons, and jets are applied independently of each other, and the shifts in  $m_t$  are extracted as uncertainties on  $m_t$ . Lepton energy or momentum scales and their uncertainties are extracted from  $Z \rightarrow 2\ell$  events in data. An additional uncertainty is estimated for jet identification by shifting the jet identification efficiency within its uncertainty in MC samples to estimate their effect on  $m_t$ . The uncertainty from modeling  $b$  tagging is evaluated by changing within their uncertainties the corrections that account for the agreement between data and MC in  $b$  tagging efficiency.

Higher-order virtual corrections to  $m_t$  are absent in the ALPGEN used to generate our standard  $t\bar{t}$  samples. We therefore compare an ensemble of pseudo-experiments using MC@NLO 3.4 [39]  $t\bar{t}$  events with one using ALPGEN events, where both employ HERWIG 6.510 [40] for modeling of hadronization. To evaluate the uncertainty associated with the modeling of initial and final-state radiation (ISR/FSR), we compare ALPGEN+PYTHIA with the renormalization and factorization scale changed up and down by a factor of 1.5 [15]. The  $\ell + \text{jets}$  analysis exhibits a discrepancy in the shape of the  $p_T$  distribution of the  $t\bar{t}$  system, which, although the dilepton statistics are limited, may be present in the dilepton sample. We evaluate the uncertainty in the modeling of the  $t\bar{t}$   $p_T$  distribution by reweighting MC events to make them match the data. The observed shift in  $m_t$  is taken as the uncertainty. Since the hadronization in our standard  $t\bar{t}$  sample is modeled with PYTHIA, we estimate a hadronization uncertainty on  $m_t$  by performing pseudo-experiments using an ALPGEN+HERWIG sample. We evaluate the effect of color reconnection by comparing  $m_t$  measurements in ALPGEN+PYTHIA samples with two PYTHIA tunes: the Perugia2011 tune that incorporates an explicit color-reconnection scheme, and the Perugia2011 NOCR tune that does not [41]. Data and MC may have different distributions in instantaneous luminosity after event selection. This uncertainty due to multiple  $p\bar{p}$  interactions is estimated by reweighting the distribution of instantaneous luminosity to make MC agree with the data for respective data-taking epochs, and then take the shift in  $m_t$  with respect to the default value. The uncertainty due to the proton structure is obtained from the 20 sets of CTEQ6L1 parton distribution functions (PDF) reweighted



to CTEQ6M, where the deviations in  $m_t$  for the 20 eigenvectors sets are added in quadrature [42].

We estimate the effect of the uncertainty on the fraction of signal or background by changing the expected  $t\bar{t}$  event yields ( $n_S$ ) up and down and the expected background yields ( $n_B$ ) down and up within their total uncertainties. The heavy-flavor scale factor, which is applied to the  $Z \rightarrow 2\ell$  cross section to correct the heavy-flavor content, is also changed up and down within its uncertainty to estimate its systematic effect on  $m_t$ .

Our templates are constructed from MC samples for  $t\bar{t}$ ,  $Z \rightarrow 2\ell$ , and diboson backgrounds, as well as data samples for instrumental background, yielding statistical uncertainties on their bin contents. We use Poisson distributions to modify bin contents within their statistical uncertainties to obtain 1000 new templates. We measure  $m_t$  in data using these templates, and the RMS of the measured top quark mass is taken as its uncertainty. Our method of  $m_t$  extraction relies on the correction of the fitted  $m_t$  to the input MC mass. The uncertainties from this calibration are applied to provide the uncertainty in  $m_t$ . The uncertainty is reduced substantially from Ref. [14] due primarily to the reduction in the uncertainty in jet energy calibration and the optimizations for improvements in statistical uncertainty. Larger MC samples also contribute by lowering statistical fluctuations on systematic uncertainties, or reducing statistically limited systematic uncertainties.

## 9. Conclusions

We have measured the top quark mass in the combined dilepton channels ( $e\mu$ ,  $ee$ ,  $\mu\mu$ ):

$$m_t = 173.32 \pm 1.36(\text{stat}) \pm 0.85(\text{syst}) \text{ GeV} \\ = 173.32 \pm 1.60 \text{ GeV}.$$

This measurement is consistent with the current world average value of  $m_t$  [18]. Our measurement is the most precise dilepton result from the Tevatron, and is competitive with the most recent LHC dilepton measurements. The systematic uncertainty of 0.49% is the smallest of all dilepton measurements.

We thank the staffs at Fermilab and collaborating institutions, and acknowledge support from the Department of Energy and National Science Foundation (United States of America); French Alternative Energies and Atomic Energy Commission and National Center for Scientific Research/National Institute of Nuclear and Particle Physics (France); Ministry of Education and Science of the Russian Federation, National Research Center “Kurchatov Institute” of the Russian Federation, and Russian Foundation for Basic Research (Russia); National Council for the Development of Science and Technology and Carlos Chagas Filho Foundation for Research Support in the State of Rio de Janeiro (Brazil); Department of Atomic Energy and Department of Science and Technology (India); Administrative Department of Science, Technology and Innovation (Colombia); National Council of Science and Technology (Mexico); National Research Foundation of Korea (Korea); Foundation for Fundamental Research on Matter (The Netherlands); Science and Technology Facilities Council and The Royal Society (United Kingdom); Ministry of Education, Youth and Sports (Czech Republic); Bundesministerium für Bildung und Forschung (Federal Ministry of Education and Research) and Deutsche Forschungsgemeinschaft (German Research Foundation) (Germany); Science Foundation Ireland (Ireland); Swedish Research Council (Sweden); China Academy of Sciences and National Natural Science Foundation of China (China); and Ministry of Education and Science of Ukraine (Ukraine).

## References

- [1] S. Abachi, et al., D0 Collaboration, Observation of the top quark, *Phys. Rev. Lett.* **74** (1995) 2632.
- [2] F. Abe, et al., CDF Collaboration, Observation of top quark production in  $p\bar{p}$  collisions with the Collider Detector at Fermilab, *Phys. Rev. Lett.* **74** (1995) 2626.
- [3] The Gfitter Group, Results for the global electroweak standard model fit, [http://project-gfitter.web.cern.ch/project-gfitter/Standard\\_Model/](http://project-gfitter.web.cern.ch/project-gfitter/Standard_Model/).
- [4] G. Aad, et al., ATLAS Collaboration, Observation of a new particle in the search for the standard model Higgs boson, *Phys. Lett. B* **716** (2012) 1.
- [5] S. Chatrchyan, et al., CMS Collaboration, Observation of a new boson at a mass of 125 GeV with the CMS experiment at the LHC, *Phys. Lett. B* **716** (2012) 30.
- [6] G. Degrandi, et al., Higgs mass and vacuum stability in the standard model at NNLO, *J. High Energy Phys.* **08** (2012) 098.
- [7] A. De Simone, et al., Running inflation in the standard model, *Phys. Lett. B* **678** (2009) 1.
- [8] F. Bezrukov, et al., The standard model Higgs boson as the inflaton, *Phys. Lett. B* **659** (2008) 703.
- [9] V.M. Abazov, et al., D0 Collaboration, Determination of the pole and  $\overline{MS}$  masses of the top quark from the  $t\bar{t}$  cross section, *Phys. Lett. B* **703** (2011) 422.
- [10] T. Aaltonen, et al., CDF Collaboration, Cross-section-constrained top-quark mass measurement from dilepton events at the tevatron, *Phys. Rev. Lett.* **100** (2008) 062005.
- [11] S. Chatrchyan, et al., CMS Collaboration, Determination of the top-quark pole mass and strong coupling constant from the  $t\bar{t}$  production cross section in  $pp$  collisions at  $\sqrt{s} = 7$  TeV, *Phys. Lett. B* **728** (2014) 496.
- [12] G. Aad, et al., ATLAS Collaboration, Measurement of the  $t\bar{t}$  production cross-section using  $e\mu$  events with  $b$ -tagged jets in  $pp$  collisions at  $\sqrt{s} = 7$  and 8 TeV with the ATLAS detector, *Eur. Phys. J. C* **74** (2014) 3109.
- [13] F. Jegerlehner, M. Kalmykov, B. Kniehl, On the difference between the pole and the masses of the top quark at the electroweak scale, *Phys. Lett. B* **722** (2013) 123.
- [14] V.M. Abazov, et al., D0 Collaboration, Measurement of the top quark mass in  $p\bar{p}$  collisions using events with two leptons, *Phys. Rev. D* **86** (2012) 051103(R).
- [15] V.M. Abazov, et al., D0 Collaboration, Precision measurement of the top quark mass in lepton + jets final states, *Phys. Rev. Lett.* **113** (2014) 032002; V.M. Abazov, et al., D0 Collaboration, Precision measurement of the top-quark mass in lepton + jets final states, *Phys. Rev. D* **91** (2015) 112003.
- [16] V.M. Abazov, et al., D0 Collaboration, Precise measurement of the top quark mass in the dilepton channel at D0, *Phys. Rev. Lett.* **107** (2011) 082004.
- [17] T. Aaltonen, et al., CDF Collaboration, Top quark mass measurement using the template method at CDF, *Phys. Rev. D* **83** (2011) 111101.
- [18] ATLAS, CDF, CMS, and D0 Collaborations, First combination of tevatron and LHC measurements of the top-quark mass, arXiv:1403.4427.
- [19] T. Aaltonen, et al., CDF Collaboration, Measurement of the top-quark mass in the  $t\bar{t}$  dilepton channel using the full CDF run II data set, arXiv:1505.00500.
- [20] G. Aad, et al., ATLAS Collaboration, Measurement of the top quark mass in the  $t\bar{t} \rightarrow \text{lepton} + \text{jets}$  and  $t\bar{t} \rightarrow \text{dilepton}$  channels using  $\sqrt{s} = 7$  TeV ATLAS data, arXiv:1503.05427.
- [21] S. Chatrchyan, et al., CMS Collaboration, Measurement of the top-quark mass in  $t\bar{t}$  events with dilepton final states in  $pp$  collisions at  $\sqrt{s} = 7$  TeV, *Eur. Phys. J. C* **72** (2012) 2202.
- [22] V.M. Abazov, et al., D0 Collaboration, The upgraded D0 detector, *Nucl. Instrum. Methods A* **565** (2006) 463.
- [23] R. Angstadt, et al., The layer 0 inner silicon detector of the D0 experiment, *Nucl. Instrum. Methods A* **622** (2010) 298.
- [24] The pseudorapidity is defined as  $\eta = -\ln|\tan(\theta/2)|$  where  $\theta$  is the polar angle relative to the proton beam direction
- [25] V.M. Abazov, et al., D0 Collaboration, Electron and photon identification in the D0 experiment, *Nucl. Instrum. Methods A* **750** (2014) 78.
- [26] V.M. Abazov, et al., D0 Collaboration, Muon reconstruction and identification with the run II D0 detector, *Nucl. Instrum. Methods A* **737** (2014) 281.
- [27] G. Blazey, et al., Run II jet physics: proceedings of the run II QCD and weak boson physics workshop, arXiv:hep-ex/0005012, 2000.
- [28] V.M. Abazov, et al., D0 Collaboration, Improved  $b$  quark jet identification at the D0 experiment, *Nucl. Instrum. Methods A* **763** (2014) 290.
- [29] V.M. Abazov, et al., D0 Collaboration, Measurement of the asymmetry in angular distributions of leptons produced in dilepton  $t\bar{t}$  final states in  $p\bar{p}$  collisions at  $\sqrt{s} = 1.96$  TeV, *Phys. Rev. D* **88** (2013) 112002.
- [30] V.M. Abazov, et al., D0 Collaboration, Jet energy scale determination in the D0 experiment, *Nucl. Instrum. Methods A* **763** (2014) 442.
- [31] M. Mangano, et al., ALPGEN, a generator for hard multiparton processes in hadronic collisions, *J. High Energy Phys.* **07** (2003) 001; M. Mangano, M. Moretti, R. Pittau, Multijet matrix elements and shower evolution in hadronic collisions:  $Wb\bar{b} + n$  jets as a case study, *Nucl. Phys. B* **632** (2002) 343; F. Caravaglios, et al., A new approach to multijet calculations in hadron collisions, *Nucl. Phys. B* **539** (1999) 215.

- [32] T. Sjöstrand, et al., High-energy-physics event generation with PYTHIA 6.1, *Comput. Phys. Commun.* 135 (2001) 238.
- [33] M. Czakon, A. Mitov, Top++: a program for the calculation of the top-pair cross-section at hadron colliders, *Comput. Phys. Commun.* 185 (2014) 2930; M. Cacciari, et al., Top-pair production at hadron colliders with next-to-next-to-leading logarithmic soft-gluon resummation, *Phys. Lett. B* 710 (2012) 612; P. Baernreuther, M. Czakon, A. Mitov, Percent-level-precision physics at the tevatron: next-to-next-to-leading order QCD corrections to  $q\bar{q} \rightarrow t\bar{t} + X$ , *Phys. Rev. Lett.* 109 (2012) 132001.
- [34] R. Brun, F. Carminati, CERN program library long writeup W5013, 1993 (unpublished).
- [35] S. Abachi, et al., D0 Collaboration, Measurement of the top quark mass using dilepton events, *Phys. Rev. Lett.* 80 (1998) 2063.
- [36] V.M. Abazov, et al., D0 Collaboration, Measurement of the top quark mass in final states with two leptons, *Phys. Rev. D* 80 (2009) 092006.
- [37] M.G. Bowler,  $e^+e^-$  production of heavy quarks in the string model, *Z. Phys. C* 11 (1981) 169.
- [38] Y. Peters, K. Hamacher, D. Wicke, Precise Tuning of the  $b$  Fragmentation for the D0 Monte Carlo, FERMILAB-TM-2425-E, 2006.
- [39] S. Frixione, et al., Single-top hadroproduction in association with a  $W$  boson, *J. High Energy Phys.* 07 (2008) 029; S. Frixione, et al., Single-top production in MC@NLO, *J. High Energy Phys.* 03 (2006) 092; S. Frixione, B. Webber, Matching NLO QCD computations and parton shower simulations, *J. High Energy Phys.* 06 (2002) 029.
- [40] G. Corcella, et al., HERWIG 6: an event generator for hadron emission reactions with interfering gluons (including supersymmetric processes), *J. High Energy Phys.* 01 (2001) 010.
- [41] P. Skands, Tuning Monte Carlo generators: the Perugia tunes, *Phys. Rev. D* 82 (2010) 074018; P. Skands, Tuning Monte Carlo generators: the Perugia tunes, arXiv:1005.3457, 2011.
- [42] J. Pumplin, et al., New generation of parton distributions with uncertainties from global QCD analysis, *J. High Energy Phys.* 07 (2002) 012.